Review

^{1}H and ^{195}Pt NMR Study of the Parallel Two-Chain Compound Per$_2$[Pt(mnt)$_2$]

Elizabeth L. Green [1],†, Lloyd L. Lumata [2], James S. Brooks [1],*, Phil Kuhns [1], Arneil Reyes [1], Stuart E. Brown [3] and Manuel Almeida [4]

[1]   Department of Physics and National High Magnetic Field Laboratory, Florida State University, Tallahassee, FL 32310, USA; E-Mails: elg11d@my.fsu.edu (E.L.G.); kuhns@magnet.fsu.edu (P.K.); reyes@magnet.fsu.edu (A.R.)

[2]   UT Southwestern Medical Center, 5325 Harry Hines Blvd., NE 4.2, Dallas, TX 75390, USA; E-Mail: Lloyd.Lumata@utSouthwestern.edu

[3]   Department of Physics and Astronomy, University of California, Los Angeles, CA 90095, USA; E-Mail: brown@physics.ucla.edu

[4]   Department of Chemistry, IST/ITN, Technical University of Lisbon / CFMCUL, Estrada Nacional n° 10, Sacavém P-2686-953, Portugal; E-Mail: malmeida@itn.pt

†   Present Address: Hochfeld-Magnetlabor Dresden, Dresden 01314, Germany.

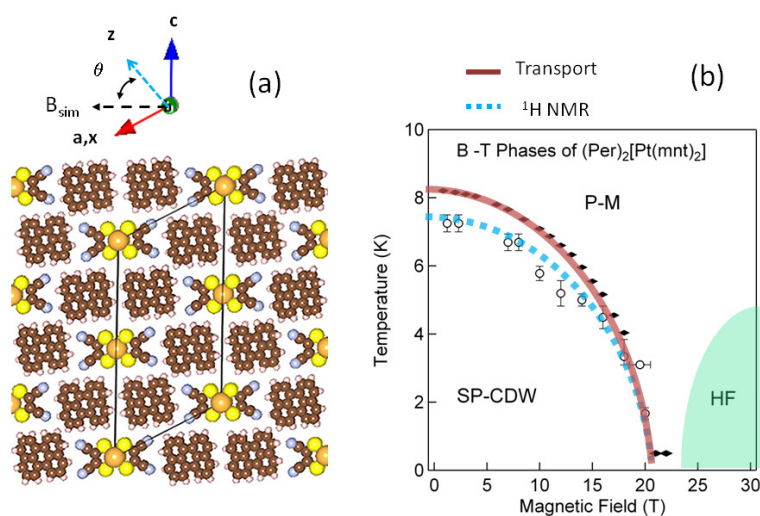*   Author to whom correspondence should be addressed; E-Mail: jbrooks@fsu.edu; Tel.: +1-850-644-2836; Fax: +1-850-644-5038.

Abstract: ^{1}H and ^{195}Pt NMR are used to probe the spin ½ anion chain in the quasi-one-dimensional conductor Per$_2$[Pt(mnt)$_2$], which exhibits nearly simultaneous charge density wave (CDW) and spin-Peierls (SP) transitions at low temperatures ($T_c \sim 8$ K). Below T_c the [Pt(mnt)$_2$] chain forms a spin-singlet state that is evident in ^{1}H NMR spectra and spin relaxation ($1/T_1$) rates; however minority unpaired Pt spins may remain in the SP ground state. With increasing magnetic field, the SP and CDW order parameters decrease in unison, indicating they are coupled up to a critical field $B_c \sim 20$ T. Above B_c, the spin singlet evolves into a spin-polarized configuration. The ^{195}Pt NMR signals vanish as either T_c or B_c are approached from within the SP ground state, suggesting the hyperfine field of the Pt nucleus is significantly stronger than at the proton sites. Simulations yield a consistent picture of the angular, temperature, and magnetic field-dependent spectral features.

Keywords: organic conductor; spin-peierls transition; charge density wave; nuclear magnetic resonance; high magnetic fields

---

1. Introduction

Two-chain quasi-one-dimensional conductors in the series $Per_2[M(mnt)_2]$ (Per = perylene; M = Au, Pt, Pd, Co, *etc*.) have long been studied due to the unique nature of their parallel, interacting chain structure [1]. Here stacks of planar perylene donors with pi-overlapped orbitals yield a highly one dimensional, electrically conducting chain in parallel with stacks of $[M(mnt)_2]$ acceptors (Figure 1a). The former exhibits a Peierls (CDW-charge density wave) transition at low temperatures, and the latter exhibits spin-Peierls (SP) transition in the case where there is a localized d-electron spin on the $[M(mnt)_2]$ site for M = Pt, Pd, *etc*. A remarkable feature of the compounds with spin on the $[M(mnt)_2]$ site is that these two transitions appear to be nearly, or even exactly coincident at a temperature T_c, giving rise to the still open question of how the order parameters couple, and which one drives the other [2,3].
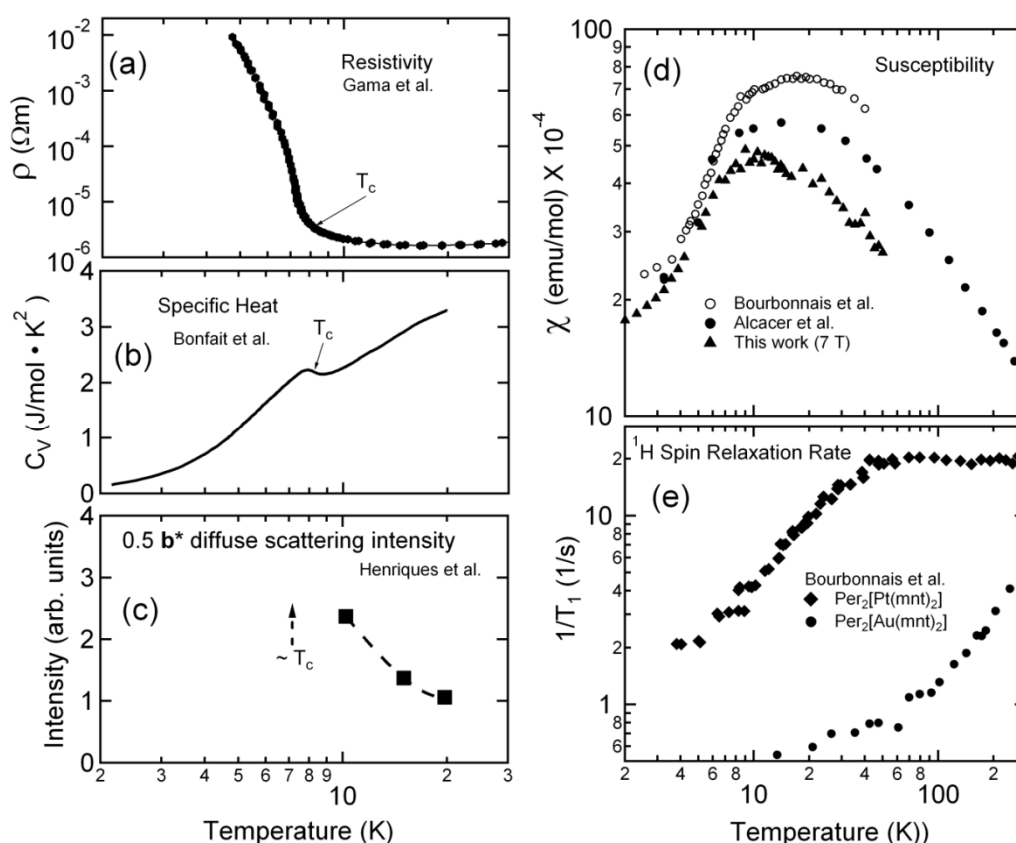
Figure 1. (**a**) View of $Per_2[Pt(mnt)_2]$ crystal structure along the stacking b-axis. In the **xyz** crystallographic coordinate system **x//a** and **y//b**. B_{sim} refers to the high-symmetry field direction ($\theta = 67°$) used in the ^1H spectra simulations. The unit cell connects the centers of the Pt sites on the $[Pt(mnt)_2]^-$ anion. The closest Pt-proton distance is 4.808 Å and the closest Pt-Pt distance is 4.125 Å (along the b-axis); (**b**) Schematic B-T phase diagram of $Per_2[Pt(mnt)_2]$ showing the spin-Peierls (SP), charge density wave (CDW), P-M (paramagnetic-metallic), and HF (high field) phase boundaries derived from the onset of splitting of NMR spectra (open symbols) and metal-insulator transitions from electrical transport measurements (solid symbols) for a field applied along the a-axis direction. (See References [4,5] for detailed discussion).

The subject of the present work is the compound $Per_2[Pt(mnt)_2]$ with a localized spin ½ on the Pt site, with the emphasis on using NMR to probe the behavior of the spin chain in the paramagnetic

and SP phases. An overview select physical properties of $Per_2[Pt(mnt)_2]$ are shown in Figure 2. Specific heat [6], electron spin resonance [2], and electrical transport [7,8] indicate a common transition in the range $T_c \sim 6$ to 8 K, and diffuse X-ray studies [9], although not below 10 K, indicate the onset of dimerization in the $[Pt(mnt)_2]$ chains. (In compounds such as M = Pd with a higher transition temperature, X-ray measurements clearly show tetramerization in the perylene chains and dimerization in the $[Pd(mnt)_2]$ chains at T_c [9], and internal consistency among the different measurements and compounds $Per_2[M(mnt)_2]$ indicate this should also be the case for $Per_2[Pt(mnt)_2]$). The periodicities of the CDW and SP chains, $q_{Per} = \pi/2b$ and $q_{Pt} = \pi/b$, are approximately commensurate with b, the lattice constant along the chains.

Figure 2. Selected temperature dependent physical properties of $Per_2[Pt(mnt)_2]$. (**a**) Resistivity in vicinity of metal-insulator transition T_c (data from Reference [10]); (**b**) Specific heat showing a jump at magnetic transition due to Pt spins (data from Reference [6]); (**c**) X-ray scattering showing onset of the diffuse 0.5 b* peak approaching T_c (data from Reference [11]); (**d**) Magnetic Susceptibility from three different studies (data from Reference [2,12] and this work); (**e**) Comparison of ^{1}H spin relaxation rates for M = Pt and M = Au materials (data from Reference [2]).

In recent years there have been extensive studies of electrical transport in $Per_2[Pt(mnt)_2]$ in magnetic fields where the resistance of the sample yields information about how the CDW ground state changes with field and temperature [7], and B-T phase diagrams have been produced that show the CDW is suppressed at high magnetic fields (~20 T at 1 K), but a new type of insulating state appears at higher fields [4,13]. Since similar studies of the spin-zero isostructural compound

Per$_2$[Au(mnt)$_2$] show that significantly larger fields (~30 T at 1 K) are necessary to suppress the conventional CDW ground state [14], one can reasonably ask what role the spin −½ chain plays in altering the B-T phase diagram, and if and how the spin and conducting chain order parameters couple. Since electrical transport is not directly sensitive to the magnetic structure in the [Pt(mnt)$_2$] chains, proton (^{1}H) and platinum (^{195}Pt) nuclear magnetic resonance (NMR) over a broad range of temperature and magnetic field has been employed to try to elucidate these questions.

In this Review, we first survey the relevant results of previous NMR studies. We next present results of ^{1}H NMR spectra which provide important information about B-T phase boundaries, and the behavior of the spin chains in the paramagnetic and spin-Peierls states. One important result is the observation that the CDW and SP order parameters remain coupled up to the critical field (~20 T) at low temperatures (see also [5]). Simulations of the spectra are described that yield a consistent picture of the angular, temperature, and magnetic field-dependent spectral features in terms of an effective dipole moment that is temperature and magnetic field-dependent. The ^{1}H spin-relaxation data are then presented. These results show evidence for a minority concentration of unpaired spins in the spin-Peierls state, the effects of which are suppressed with increasing field. We next present the results of ^{195}Pt NMR which is only measurable within the SP-CDW phase boundary. Unlike the ^{1}H NMR, in this case the ^{195}Pt nuclear spin of interest is on the same site as the d-electron spin, and this has a dramatic effect on the spectra and the relaxation rates. Finally, we put our results in the context of the problems of competing order parameters, and make conclusions and suggestions for future work. Additional details of the ^{195}Pt and ^{1}H studies are given in the Theses of Lumata [15] and Green [16] respectively.

2. Background

The primary thrust of the work reported here concerns NMR (both spectra and spin-relaxation) on single crystal Per$_2$[Pt(mnt)$_2$] with a focus on the high magnetic field (2 to 33 T) dependence of the SP-CDW phases at low temperatures, and also on the spectra over broad range of temperature above the SP-CDW ground state. Earlier however, a milestone in the understanding of the magnetic properties of the Per$_2$[Pt(mnt)$_2$] system in the higher temperature paramagnetic phase is the work of Bourbonnais *et al.* [2] which addressed the temperature dependence of the ^{1}H spin relaxation rate $1/T_1$ at 0.855 T from room temperature to ~ 4.2 K in a powdered sample. This group also measured $1/T_1$ in the zero-spin anion analogue Per$_2$[Au(mnt)$_2$], and combined with results of the magnetic susceptibility (χ) and electron spin resonance (ESR) data, affirmed the following:

(1) The susceptibility is Curie-Weiss like at higher temperatures (T > 20 K) in the paramagnetic state. The parameters are $k_B T_{SP}^0 \sim \Theta \sim J/k_B \sim \Delta k_B \sim 20$ K. From a Curie-Weiss law fit to $\chi(T)$, the effective number of Bohr magnetons $p = g[J(J + 1)]^{1/2}$ is about 1.87 [17], (close to the value $p = 1.73$ for g = 2, and J = ½). Since a dimerization driven solely by a one-chain spin-lattice effect has the criterion $k_B T_{SP}^0 \ll J$, the fact that $T_c \sim 8$ K (*i.e.*, is so high) is anomalous, and the origin of the SP state is not clear. Hence the proximity of the CDW order parameter may "aid" the formation of the SP state, as discussed below.

(2) In the paramagnetic state, the ^{1}H spin-relaxation rate in Per$_2$[Pt(mnt)$_2$] is dominated by the transverse dipolar coupling between the Pt spins and the proton sites, and follows the relationship

$1/T_1 \sim T\chi(T)$ down to about 20 K (see also Section 4). Therefore at high temperatures in the Curie limit where $\chi(T) = C/T$, $1/T_1$ is independent of temperature. The conclusion was that, in comparison with Per$_2$[Au(mnt)$_2$], the ^{1}H signal is primarily affected by the Pt spins. This opens the door to using ^{1}H NMR to monitor the spin configuration of the SP state in the [Pt(mnt)$_2$] chain *vs.* field and temperature, even though the protons sit at the periphery of the perylene molecule, at distances of 4.8 Å or more from the Pt sites. As we will see later, the situation for NMR on the [195]Pt sites is very different.

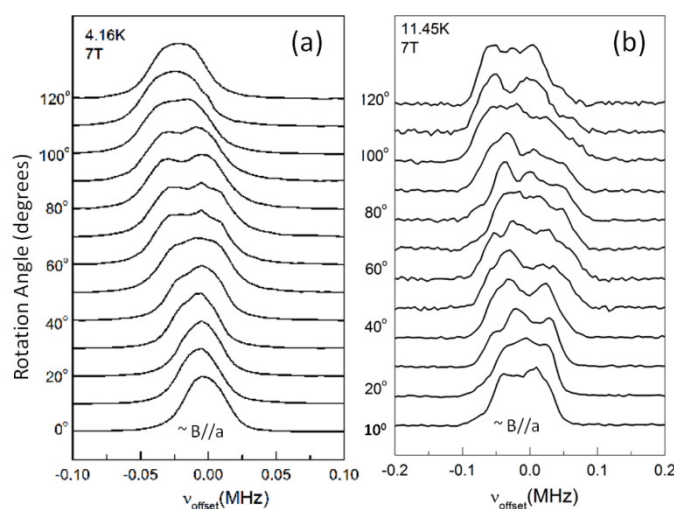Recently, we reported [5] the correspondence of the ^{1}H NMR spectra and spin-relaxation rates to the B-T phase diagram of Per$_2$[Pt(mnt)$_2$] below 10 K in fields up to 26 T. The key results of this study were that the NMR spectral line shapes underwent fundamental changes passing from the low temperature—low magnetic field singlet SP-CDW insulating ground state to the high temperature paramagnetic, metallic phase, and/or into the high magnetic field phase. By monitoring the field and temperature where the characteristic, narrow line seen in the spin singlet state started to evolve into the broader, multiple peaked spectrum characteristic of the paramagnetic state, an estimate of the SP phase boundary could be determined, and compared with previous determinations based on electrical transport. The conclusions of this work were that the formation of the CDW state is necessary to induce the SP transition, which otherwise would not form, and that the two order parameters remain coupled at least until the low temperature critical field of $B_c \sim 20$ T is reached (Figure 1b).

3. ^{1}H NMR Spectra and the SP Phase Boundary

3.1. Angular Dependent Spectra

Proton spectra *vs.* field direction are shown in Figure 3 at 7 T for 4.16 K and 11.45 K (in this work, the field is always directed in the a-c crystallographic plane).

Figure 3. Angular dependent ^{1}H NMR spectra of Per$_2$[Pt(mnt)$_2$] at 7 T. (Traces are normalized and offset for clarity; center frequency = 298.218 MHz.) The angles are with respect to a high symmetry direction where the overall linewidth is minimized, that experimentally, is approximately for field along the a-axis direction: (**a**) in the SP ground state at 4.16 K; and (**b**) in the high temperature paramagnetic state at 11.45 K.
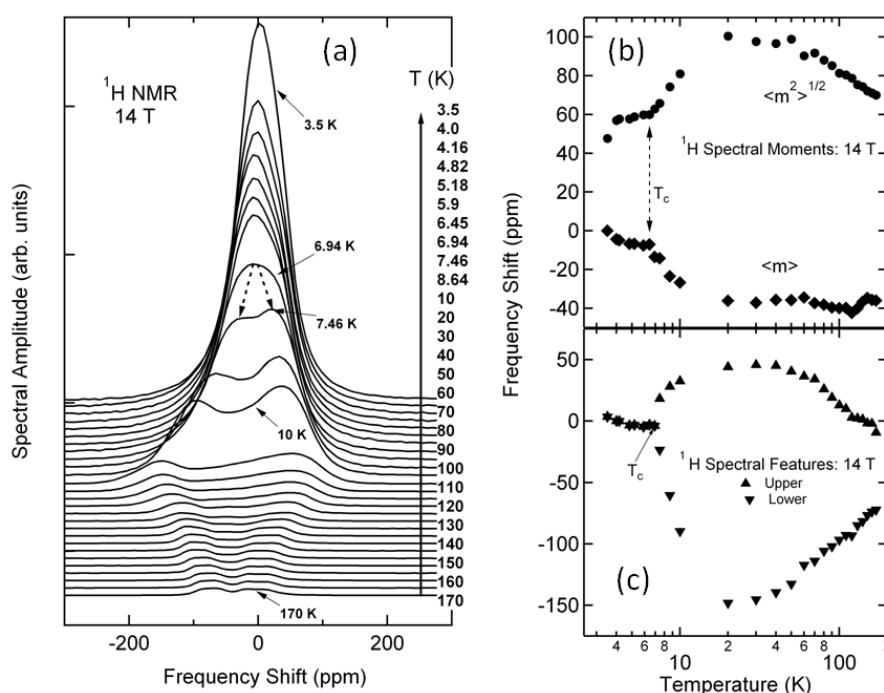
For high symmetry field directions within the SP-CDW phase (4.16 K < T$_c$), only one spectral line is evident, but as the sample is rotated in field additional spectral components appear for some directions. This effect may arise from the existence of minority unpaired spins as described in Section 4. Above the phase boundary (at 11.45 K > T$_c$) multiple peaks appear even along high symmetry directions, and the total linewidth is about twice that at 4.16 K; with rotation above T$_c$, the linewidth and the multiple peak features increase significantly. In this work we take the transition between the single and multiple peak spectra along a high symmetry direction as the indication of the transition between the singlet and paramagnetic phase with either increasing temperature or magnetic field, as discussed in the following sections.

3.2. Temperature Dependent Spectra

Proton spectra at 14 T along a high symmetry direction are shown in Figure 4a from 3.5 to 170 K.

Figure 4. (**a**) Temperature dependent ^{1}H spectra of Per$_2$[Pt(mnt)$_2$] at 14 T from 170 K to 2.5 K. (Center frequency = 596.729 MHz; see Figure 7b for simulation.) Dashed arrows indicate the transition from a single to multiple peaks in the spectrum at T$_c$. (Traces are offset for clarity; center frequency = 596.729 MHz); (**b**) Temperature dependence of computed moments <m> and <m^2>$^{1/2}$ from the 14 T spectra; (**c**) Temperature dependence of upper and lower frequency peak features.
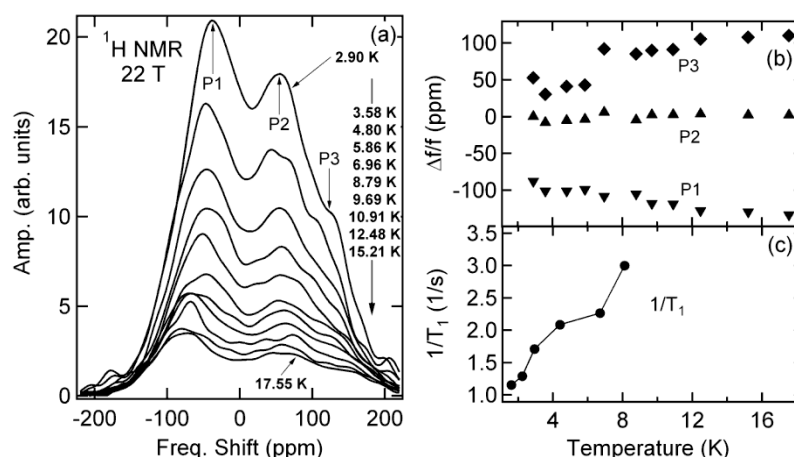

At high temperatures, there are multiple lines and with decreasing temperature the overall linewidth broadens until about 20 K, below which linewidth decreases and the spectrum collapses to a single line at the lowest temperature. In Figure 4b the first moment <m> (which is proportional to the shift $\Delta v/v_0$) and the root of the second moment <m^2>$^{1/2}$ (which is proportional to the linewidth) are shown *vs.* temperature, as computed from the data. There is a distinct change of slope in both moments at the transition T$_c$ between 6 and 7 K; likewise T$_c$ is evident as a sharp transition from a multiple to a single

line in Figure 4c, the latter taken as an estimate of the onset of the SP phase (similar results and analysis for 7 T are shown in Reference [5]). The results of Figure 4 yield additional information about the hyperfine field seen at the proton sites due to the Pt spins. First, for 170 > T > 20 K, there is a direct correspondence between the paramagnetic susceptibility and the shift of individual peaks in the multiple peak spectrum (Figure 4c) and in $<m^2>^{1/2}$ (Figure 4b). However, the temperature dependence of $<m>$ is relatively small, and difficult to determine above 20 K, but at temperatures below 20 K approaching and entering the SP ground state, it shifts significantly and approaches a constant by 3.5 K. By referencing the change in the first moment at 20 K to the low temperature value, *i.e.*, $\Delta v/v_0 = (v(20\ K) - v(3.5\ K))/v(3.5\ K)$, and using the susceptibility data of Reference [2], we find the hyperfine coupling constant at 20 K is $A_{hf} = 56$ Oe/μ_B, based on the relationship $K = A_{hf}\ \chi(T)/\mu_B N_A$ where $K = \Delta v/v_0$ and N_A is Avogadro's number. The shift K upon entering the low temperature ground state (for fields ≤ 14 T) is uniform with increasing field (or frequency), and scales with field, *i.e.*, $\Delta v/v_0 = \Delta H/H =$ constant ~ 40 ppm. This is consistent with the loss of hyperfine field in the SP spin-singlet ground state. The linewidth of the proton NMR line in the SP spin-singlet state is about $<m^2>^{1/2} = 7.8$ gauss. Like the low temperature shift in $\Delta v/v_0$ (20 K > 3.5 K), the linewidth does not appear to be strongly field-dependent up to 14 T. The maximum proton-proton hyperfine field for a separation of about 2.5 Å is about 1 gauss, so the broadening of the line in the SP ground state may arise from factors other than just isolated proton contributions.

In Figure 5 temperature dependent spectra above the main SP ground state (B > B_c) at 22 T are presented for temperatures from 2.9 to 17.55 K. The multiple peak spectra are characteristic of the paramagnetic phase. In comparison with similar spectra in incommensurate systems such as $CuGeO_4$ [18] or $(TMTTF)_2PF_6$ [19], aside from some minor changes in one of the spectral feature P3 in Figure 5b and $1/T_1$ near 5 K in Figure 5c, we find no apparent signature of a transition from an undimerized to an incommensurate (U-I) phase in $Per_2[Pt(mnt)_2]$. Although this may simply be due to the highly commensurate nature of the SP and CDW structure in this material, we currently do not have a full answer as to why the U-I phase boundary, which is seen in the other cases, is not present here.

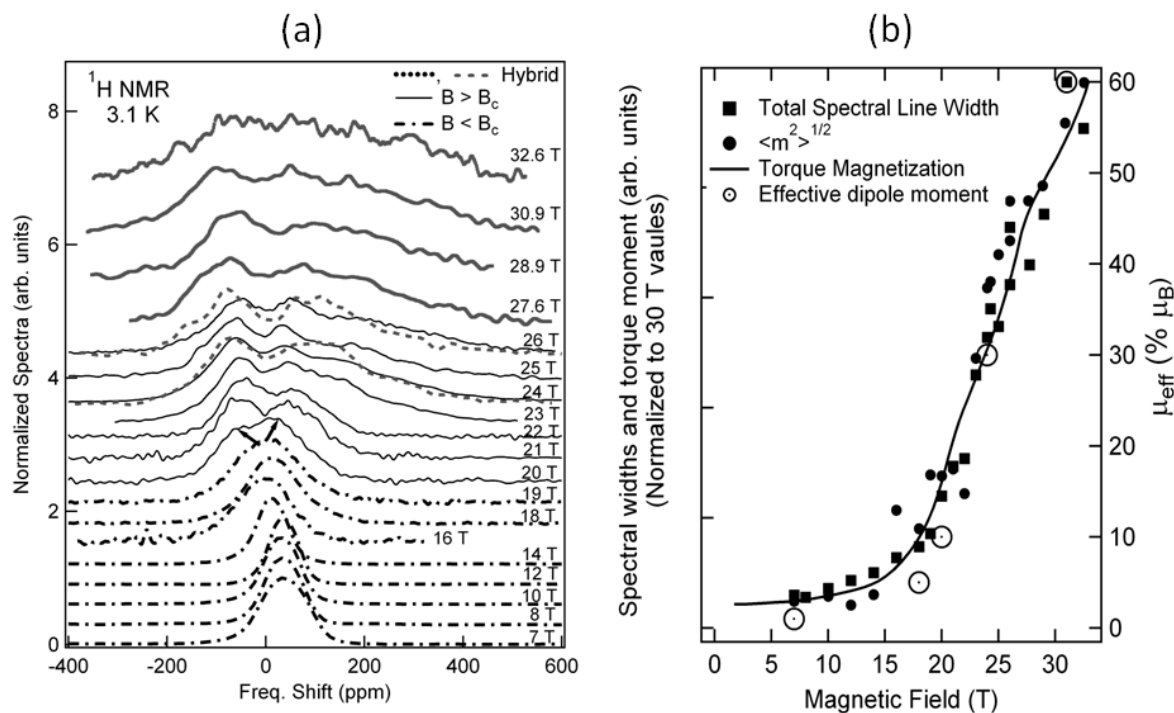**Figure 5.** (**a**) Temperature dependent ^1H spectra of $Per_2[Pt(mnt)_2]$ above the SP critical field B_c. (Center frequency = 935.95 MHz); (**b**) Temperature dependence of selected peak features; (**c**) Temperature dependence of the spin relaxation rate.

3.3. Magnetic Field Dependent Spectra

The evolution of the proton spectra at low temperatures (3.1 K) up through the critical field is shown in Figure 6a. The data is a combination of superconducting, resistive magnet, and Hybrid magnet experiments. At low fields, the single line characteristic of the spin singlet SP phase remains relatively unchanged until about 14 T where it starts to shift to lower frequency. This is the same $\Delta\nu/\nu_0$ shift (~40 ppm) seen in the crossing of the phase boundary for the temperature dependent data at 14 T. Between 19 and 20 T, the line splitting (see arrows) characteristic of a transition to a paramagnetic phase is evident. Taken together, the spectral splitting in both the temperature dependent and field dependent data provide the B-T phase boundary of the SP phase for comparison with that obtained for the CDW phase from transport studies as shown in Figure 1b.
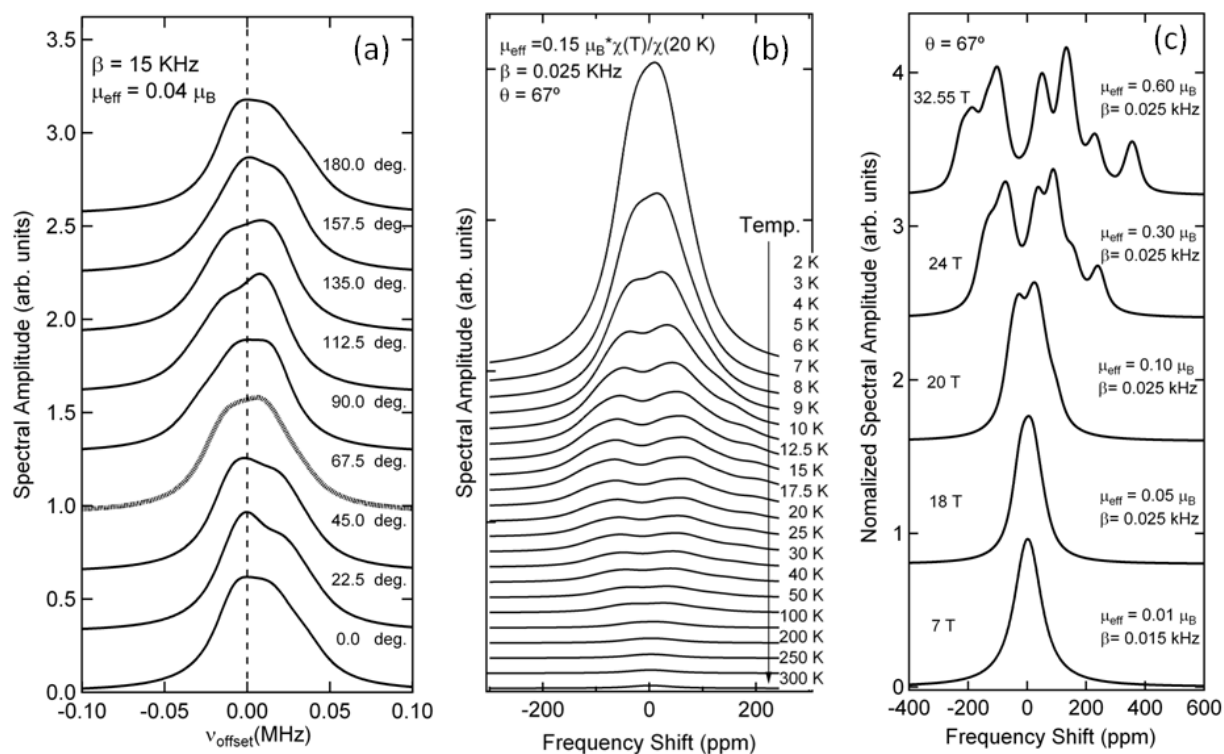
Figure 6. (**a**) Summary of field dependent ^{1}H spectra of Per$_2$[Pt(mnt)$_2$] at 3.1 K from the SP ground state into the high field phase above B$_c$. Arrows represent spectral splitting between 19 at 20 T. (Traces are normalized and offset for clarity; center frequencies set to γ_0B; see Figure 7c for simulation); (**b**) Left axis: comparison of linewidths in (**a**) (from second moment analysis and full spectral width) with previous torque magnetization data [4]. Right axis: magnetic field dependence of values of μ_{eff} used to fit the simulated spectral widths to the data in (**a**). (All values normalized to a common scale for comparison).

Above 14 T, $<m^2>^{1/2}$ begins to broaden with increasing field, and in Figure 6b a comparison is made with magnetic torque data [4]. Here the implication is that the spin-Peierls singlet ground state is being broken, and field-induced unpaired spins begin to dominate the magnetic properties. A connection to the increase in the effective dipole moment (circles in Figure 6b) with increasing field is discussed in the next section.

Figure 7. Computed ¹H spectra (traces offset for clarity) from Equation (4) for single crystal Per$_2$[Pt(mnt)$_2$] *vs.* (**a**) field direction; (**b**) temperature; and (**c**) magnetic field/effective dipole moment: μ_{eff} and β for each magnetic field shown was adjusted to fit the simulated spectra to the experimental spectra in Figure 6a (μ_{eff} *vs.* B values are plotted in Figure 6b).

3.4. Computed ¹H Spectra in the Paramagnetic Phase

We have used a simple dipolar model to estimate the ¹H NMR spectra in the paramagnetic phase of Per$_2$[Pt(mnt)$_2$] outside the SP phase boundary. The input into the model includes a real-space representation of the positions of the proton and platinum atoms in the crystal structure, using a 3-D crystal array with approximately 410 unit cells, derived from a standard *cif* file in *xyz* (Cartesian) format (Figure 1a). We use the standard vector dipolar expression to find the magnetic field due to a Pt site:

$$\mathbf{B}_{ij}(\mathbf{r}_{ij}) = [(3\boldsymbol{\mu}_{eff}\cdot\mathbf{r}_{ij})(\mathbf{r}_{ij}/r_{ij}) - \boldsymbol{\mu}_{eff}]/r_{ij}^3 \qquad (1)$$

where $\mathbf{r}_{ij}$ is the vector distance between a proton at position i and a Pt spin at position j; and $\boldsymbol{\mu}_{eff}$ is the effective Pt electron moment in the solid state. In this expression, we assume the paramagnetic moment is always directed along the applied field, *i.e.*, $\boldsymbol{\mu}_{eff}//\mathbf{B}_{ext}$, and that only the component of the dipole field parallel to the applied field $\mathbf{B}_{ij}\cdot\mathbf{B}_{ext}/B_{ext}$ contributes to the resonance. Each proton, due to the many inequivalent positions in the crystal, will contribute one component to the total spectrum at frequency $\omega_i = 2\pi\gamma\sum_j\mathbf{B}_{ij}\cdot\mathbf{B}_{ext}/B_{ext}$ (neglecting Lorentz and demagnetization terms). The time-dependent signal from the ensemble will then be:

$$S(t) = \sum_i \exp(-i\omega_i t) \exp(-\beta_i t) \qquad (2)$$

where β_i is the damping factor at proton site *i*. S(t) can be Fourier transformed to obtain the frequency dependent spectrum, *i.e.*,

$$A(\omega) = \int_{-\infty}^{\infty} \sum_i \exp(-i\omega_i t) \exp(-\beta_i t) \, dt \tag{3}$$

which can be integrated, under the assumption that $\beta_i = \beta$ is the same at all proton sites, as:

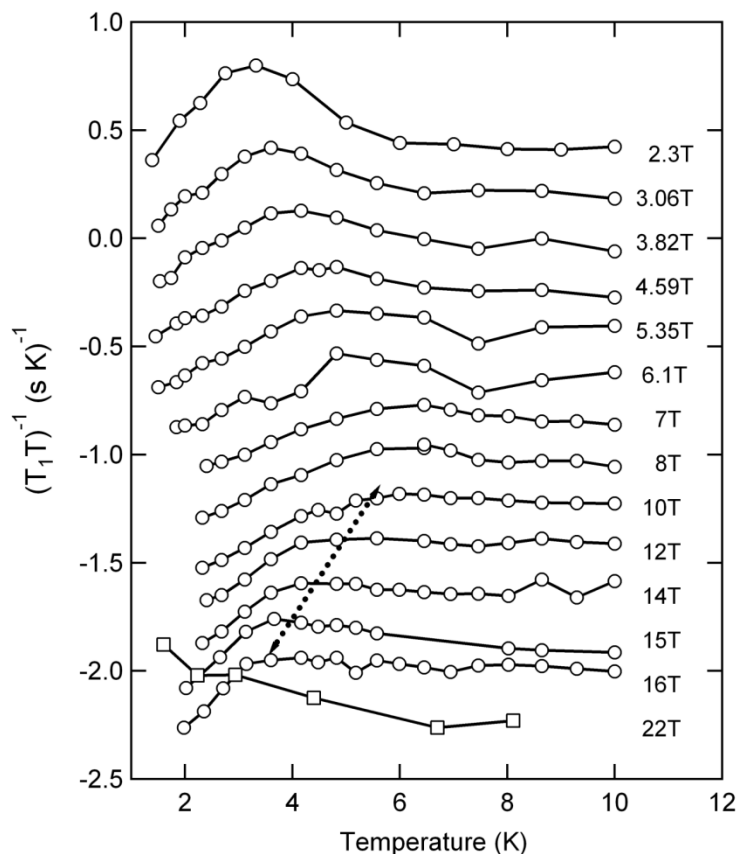$$A(\omega) = \sum_i \beta_i/[(\omega - \omega_i)^2 + \beta^2] \tag{4}$$

Implicit in the formulation above is the angular dependence of the spectrum with respect to the field and crystalline axis directions, as well as the temperature and magnetic field dependence of the spectrum through μ_{eff}. In Figure 7a, we compute the angular dependent spectrum for $\mu_{eff} = 0.04 \ \mu_B$ and $\beta = 15$ kHz, corresponding to Figure 3a for 4.16 K: although the experiment is in the SP ground state, the small values of μ_{eff} and β represent the presence of minority unpaired spins in the crystal lattice, and therefore the spectrum will have multiple peaks with field rotation. In Figure 7b we have computed the temperature dependent spectrum for magnetic field $\mathbf{B}_{sim}$ along a high symmetry axis $\theta = 67°$ (see Figure 1a), based on a maximum effective moment $\mu_{eff} = 0.15 \ \mu_B$ at 20 K, weighted by the temperature dependent susceptibility at 7 T. The computed spectrum, adjusted for the Boltzmann factor T^{-1}, has the qualitative features of the experimental spectrum shown in Figure 4a. In Figure 7c the magnetic field dependence of the paramagnetic spectrum (again for $\theta = 67°$) is shown at constant temperature, where we have modeled the field dependence in terms of an increase of μ_{eff} with field by matching the simulation linewidths with the experimental linewidths from Figure 6a for selected fields. For comparison we have plotted these simulation μ_{eff} values *vs*. magnetic field in Figure 6b, where we find the scaling to be very consistent with the linewidth and magnetic torque data. It is clear that at high fields (of order 50 to 60 T) μ_{eff} will eventually approach the full Bohr magneton μ_B in a fully polarized state.

The calculation shows that: (i) the multiple peaks in the paramagnetic phase are due to the in-equivalent proton sites; (ii) even in the SP state at low temperatures there are residual features of multiple peaks in the spectra indicating that the spin-singlet dimerized state may not be complete, which is consistent with the findings of $1/T_1$ and χ that suggest that there are still unpaired spins at low temperatures as discussed in the next section; (iii) the larger the effective moment is, the more pronounced the multiple peaks are, and the broader the linewidth.

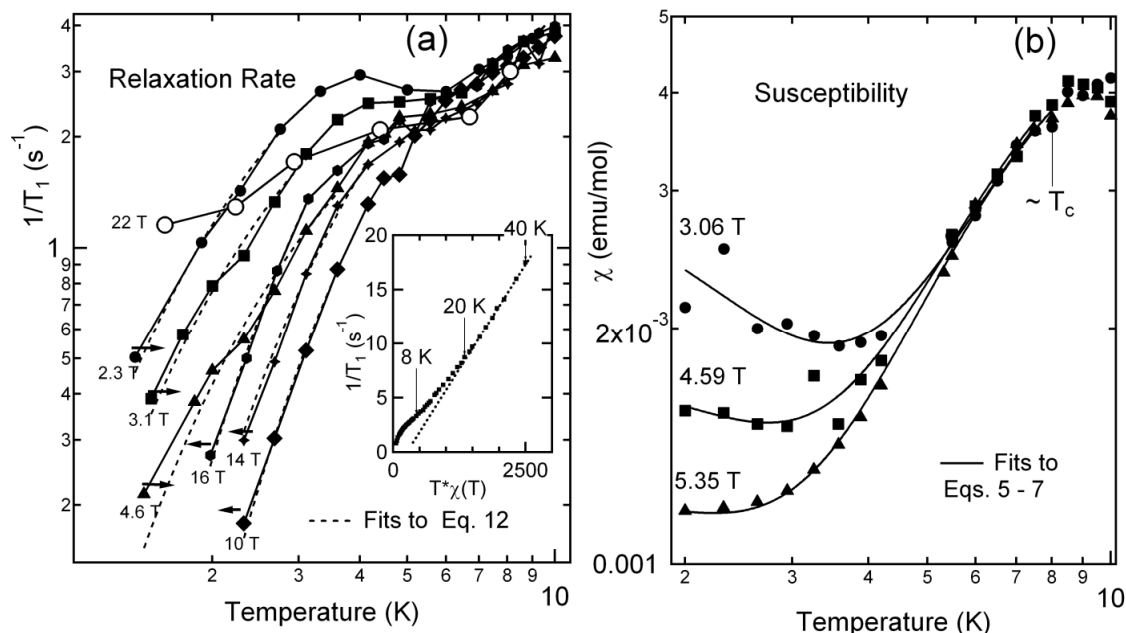## 4. Magnetic Field and Temperature Dependent ^{1}H Spin-Relaxation Rates $1/T_1$

The nuclear spin relaxation rate $1/T_1$ yields information complementary to the spectra. In Figure 8 the spin relaxation rate *vs*. temperature for increasing magnetic field is shown in terms of the Korringa relationship for a metal $1/T_1T = $ constant, giving a convenient point of reference for the temperature dependence of the relaxation data.

Figure 8. Summary of temperature and field dependent spin-relaxation rates of Per$_2$[Pt(mnt)$_2$] in terms of $1/T_1T$. Data at 2.3 T is not offset, but subsequent curves are incrementally offset by -0.2 (s K)$^{-1}$ for increasing magnetic field. The dashed line refers to "dog-leg" feature in the relaxation data that appears above 10 T.

We note that over the narrow range of temperature above T_c where the data extend, one cannot discriminate between $1/T_1 \sim T\chi(T)$, the Korringa relationship, or other possible dependences of $1/T_1$ on temperature (see also inset of Figure 9a and discussion below). The data in Figure 8 show some unusual features. First is the rise in $1/T_1T$ at or below the temperature T_c. This rise eventually is suppressed above 10 T. This feature is not apparent in, for instance, the case of CuGeO$_4$ where for NQR measurements, $1/T_1$ drops monotonically with temperature, and shows a "dog-leg" type feature at the undimerized to dimerized (U-D) phase boundary [18]. (However, in magnetic field, NMR does show some deviation from the NQR data in the CuGeO$_4$ transition region.) The correspondence between the field dependent data in Figure 8 and the B-T phase boundary is not as clear as it is for the spectral line shape changes, due in part to the anomalous rise in $1/T_1$ at lower fields below T_c. Above 10 T however, the anomalous rise is suppressed, and the SP phase transition is more apparent where a "dog-leg" feature (dashed line) moves to lower temperature with increasing field. Second, at lower temperatures the slope of $1/T_1T$ drops monotonically in temperature for all fields below the critical field of 20 T. However, the slope in the low temperature limit is not monotonic in field, and reaches a minimum in the range 7 to 10 T. Above the critical field, in the high field phase region, the behavior of $1/T_1T$ shown for 22 T is clearly very different.

Figure 9. (**a**) Temperature dependence of $1/T_1$ for $Per_2[Pt(mnt)_2]$ at different magnetic fields. Arrows refer to direction of curves for increasing magnetic field. Inset: test of relationship $1/T_1 \sim T*\chi(T)$ showing deviation below 20 K (dashed line). Inset data is from Reference [2]; (**b**) Susceptibility *vs.* temperature for selected magnetic fields.

The non-monotonic field dependence of the low temperature $1/T_1$ data is best examined by plotting $1/T_1$ directly against T (Figure 9a), where, for comparison, we also juxtapose susceptibility data at available corresponding magnetic fields (Figure 9b).

For a given temperature below 3 K, $1/T_1$ decreases with increasing field up to 10 T, but above 10 T it begins to increase. Correspondingly, in the susceptibility data we note that in addition to the drop in $\chi(T)$ due to the onset of the SP gap, there is a "Curie tail" at low temperatures which diminishes with increasing field. These results indicate the presence of two opposite, field-dependent mechanisms that manifest themselves in χ and $1/T_1$. The field dependent paramagnetic susceptibility for a spin $-\frac{1}{2}$ system is described by the Brillouin function, where for $J = \frac{1}{2}$ simplifies to

$$\chi_p(T) = (N_p\mu_B/B)\,\tanh(x) \tag{5}$$

(See Kittel [20]: here N_p is the number of paramagnetic spins and $x = \mu_B B/k_B T$ and $p = g(J(J + 1))$ is implicit). The Curie tail may be ascribed to a population (N_p) of unpaired spins. The so called "impurities" Curie tail corresponding up to about 3% of the total spin population has been always found in different $Per_2[Pt(mnt)_2]$ samples to a larger or smaller extent. This tail is common in 1D spin chain systems (e.g., [21,22]) and it believed to correspond to defects (missing molecules) or staking defaults of any kind, rather than impurities. In the present case it is the anions $[Pt(mnt)_2]$ which remain unpaired. This has been confirmed by EPR [23] which shows in single crystals that this tail corresponds to a signal with g-values typical of $[Pt(mnt)_2]^-$. Following Bourbonnais *et al*. [2] the contribution to the susceptibility from the Pt spins (N_{SP}) involved in the dimerization will be only from those spins excited across the effective spin-Peierls gap Δ. Treating these spins also as a paramagnetic contribution as in Equation (5) leads to the following expression for $\chi_{sp}(T)$ below $T_{SP\text{-}CDW}$:

$$\chi_{sp}(T) = (N_{SP}\mu_B/B) \tanh(x)\exp(-\Delta/k_B T) \tag{6}$$

Therefore, the total susceptibility below $T_{SP\text{-}CDW}$ may be written as:

$$\chi(T) = \chi_{sp}(T) + \chi_p(T) \tag{7}$$

The data in Figure 9b below $T_c \sim 7$ K were fitted accordingly to Equations (5–7) and yielded the following fitting parameters, namely $N_{sp}/N \sim 97.5\%$ and $N_p/N \sim 2.5\%$ (where $N = N_{sp} + N_p$), and $\Delta/k_B = 18.3 \pm 1.1$, 17.2 ± 0.71, and 15.9 ± 0.34 K for magnetic fields 3.06, 4.59, and 5.35 T respectively.

We next turn attention to the temperature and field-dependent spin relaxation data in Figure 9a, where below 3 K $1/T_1$ is thermally activated. We note that the relationship $1/T_1 \sim T\chi(T)$ is not valid below about 20 K as shown in the Figure 9a inset. In the mean field description, and supported by previous transport studies [7], the effective spin Peierls gap follows the general relationship:

$$\Delta(B) = \Delta(0)*(1 - (B/B_c)^2) \tag{8}$$

where B_c is the upper critical field; and $\Delta(0)$ is the gap for $B = 0$. ($\Delta(B)$ is also temperature dependent near the phase boundary, but we have neglected this in the present analysis which focuses on the data in the low temperature limit) Following a simple model for the relaxation rate of the spin-Peierls system $1/T_1^{SP}$ in terms of an activated behavior with energy $\Delta(B)$ we would expect the relationship:

$$1/T_1^{SP} = \Gamma \exp(-\Delta(B)/k_B T) \tag{9}$$

where Γ is an intrinsic inverse lifetime [18]. Since the slopes of $1/T_1$ *vs.* T below 3 K are activated, and proportional to an effective energy gap, the fact that they are not monotonic in field implies the interplay of two, field dependent energy gaps that influence $1/T_1$. Indeed, only above 10 T does Equation (9) appear to be operative. Recalling the implied presence of unpaired spins from the low temperature, field dependent Curie tail, we may further add to the total relaxation rate a paramagnetic term:

$$1/T_1^{P} = \Pi \exp(-p\mu_B B/k_B T) \tag{10}$$

Here Π represents the inverse lifetime of the paramagnetic background, and in this case the Zeeman energy $p\mu_B B$, where p is an effective Bohr magneton number, plays the role of the energy gap. Hence the total relaxation rate is:

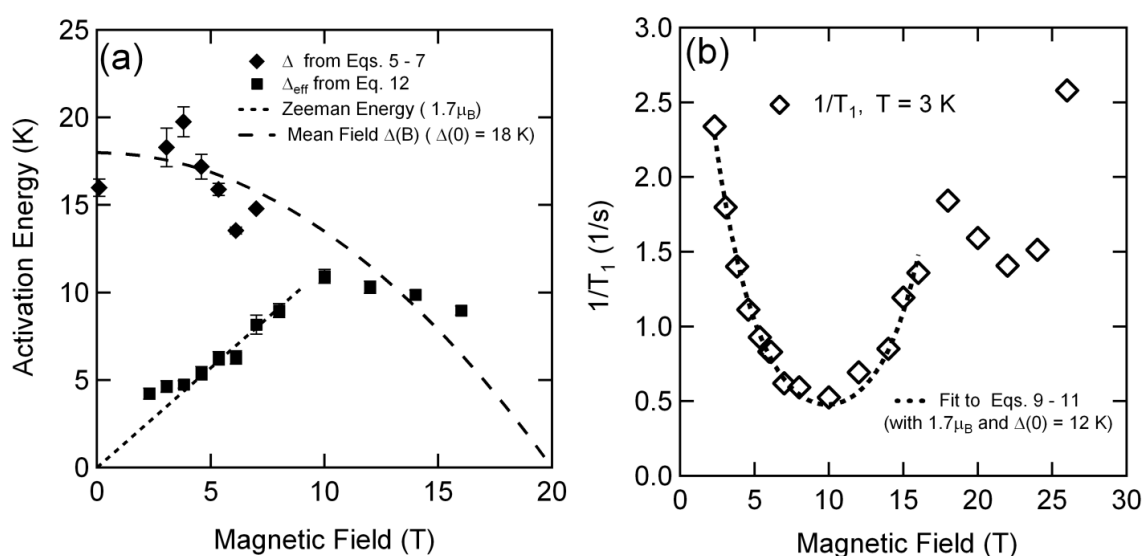$$1/T_1 = 1/T_1^{P} + 1/T_1^{SP} \tag{11}$$

By inspection, it is evident that Equation (10) will dominate the behavior of $1/T_1$ when the Zeeman energy (*i.e.*, field) is low, and that as the Zeeman energy increases with field, eventually the mean field SP gap which decreases with field will determine $1/T_1$ (Equation (9)). We found that a fit of Equation (11) to the data is difficult, since the parameters Γ and Π have, in addition to the Zeeman and SP gap, some field and temperature dependence. To obtain a general description of $1/T_1$, we have used the effective expression:

$$1/T_1 = W \exp(-\Delta_{eff}/k_B T) \tag{12}$$

where W is an effective inverse lifetime to derive an effective activation energy Δ_{eff} over the entire field range below B_c by fitting the $1/T_1$ data. We note that $\Delta_{eff} \sim p\mu_B B/k_B$ in the low field limit, and $\Delta_{eff} \sim \Delta(B)$ in the high field limit.

This is evident in Figure 10a where there is a crossover from Zeeman to mean-field gap behavior at around 10 T. Returning now to Equations (8–11), we may fit the field dependence of $1/T_1$ at a constant temperature of 3 K with the parameters $p\mu_{Beff}$ = 1.4 μ_B (dashed line in Figure 10a) and a field dependent mean field gap with $\Delta(0)/k$ = 12 K (solid line in Figure 10a), as shown in Figure 10b. Due to the many parameters and experimental uncertainties, this "two-spin" model analysis is only semi-quantitative, but captures the main features of the spin relaxation behavior at constant temperature below B_c. We close this section by noting that near 20 T, $1/T_1$ shows evidence for a phase transition (Figure 10b). It is possible that features associated with sub-phases in the high field state seen in transport and magnetization [4] may appear in $1/T_1$ (such as the dip between 20 T and 25 T, but more detailed work will be needed to resolve this. The increase at higher fields above 25 T may be the result of an increase in paramagnetic spins due to the further destruction of the spin-singlet chains, which may still be breaking down above the critical mean field B_c.

Figure 10. (**a**) Effective gap parameters for Per$_2$[Pt(mnt)$_2$] derived from spin-relaxation and susceptibility analysis. Error bars represent uncertainties in fitting parameters for specific data sets. Overall uncertainties between fits to all data sets, which are significantly larger, are manifested by the scatter in the fit parameters; (**b**) Spin-relaxation rates from ^{1}H NMR *vs.* field at 3.1 K, fit to Equation (11) below B_c.
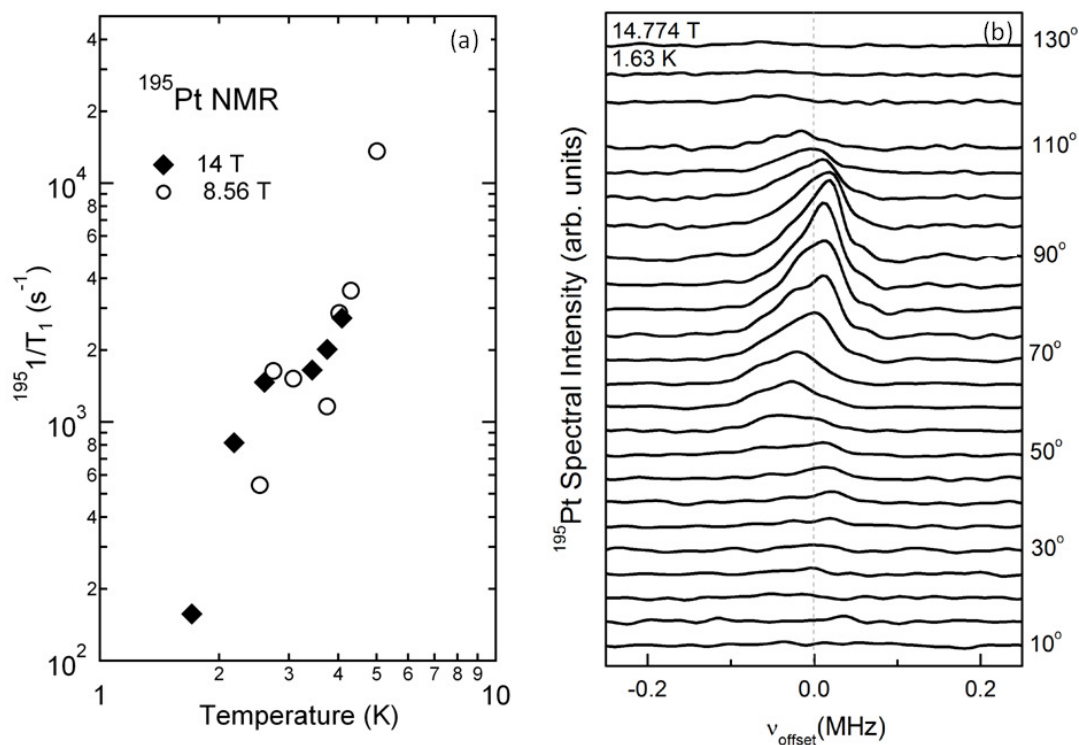

5. ^{195}Pt NMR below the SP-CDW Phase Boundary: Relaxation and Spectral Features

We initiated our study of the SP chain behavior in Per$_2$[Pt(mnt)$_2$] with ^{195}Pt NMR (γ = 9.14894 MHz/T). A fundamental difference between ^{1}H NMR described above and ^{195}Pt NMR is that in the latter case, the NMR nucleus is at the center of the electronic orbital that gives rise to the dipolar field. In the former case, the NMR nuclei (protons) are separated on average by about 10 Å from the d-electron spins.
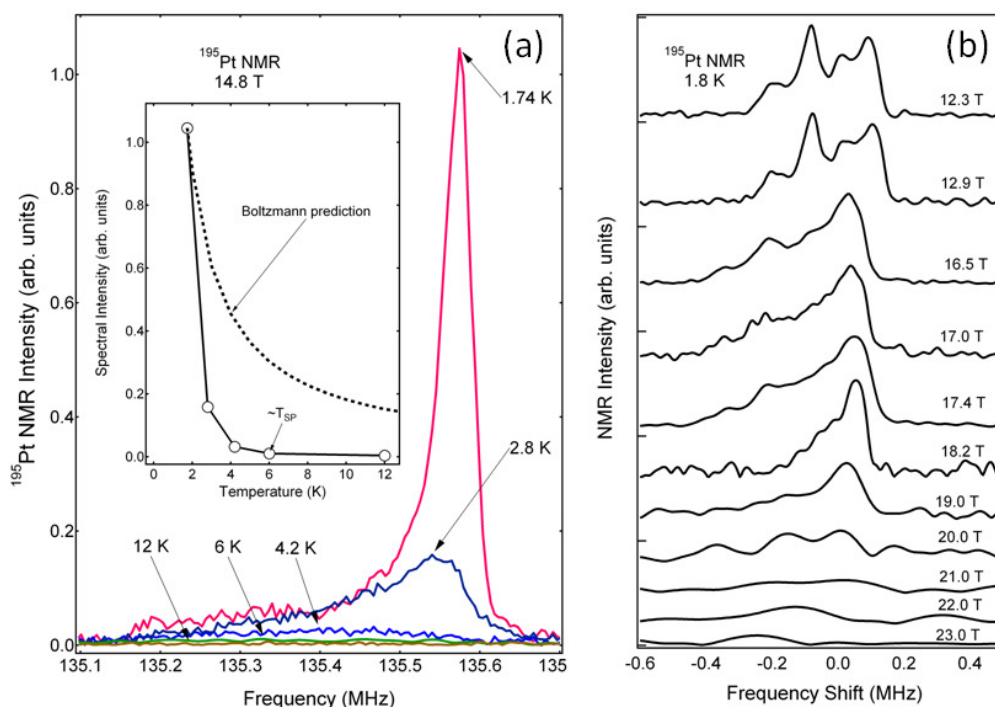
This became evident in a preliminary study of the spin-relaxation time, shown in Figure 11a. Here, we note that in the SP phase $1/T_1$ is on average 1000 times faster on the Pt nuclear site than on the proton site; and in this study $1/T_1$ was too fast to measure in the paramagnetic state at higher temperatures. Our results on ^{195}Pt NMR were therefore restricted to low temperatures, and as shown

below, also to fields below 20 T. The angular dependence on a single crystal (Figure 11b—rotation in the a-c plane) for 14.774 T at 1.63 K indicated a hyperfine field anisotropy of about 740 ppm, substantially larger than that for ^{1}H NMR shown in Figure 3a, which is only about 8.5 ppm. The attenuation of the spectral amplitude for certain directions may arise from the anisotropy in B_c [4], coupled with the severe attenuation of the ^{195}Pt NMR signal near B_c as discussed below. To obtain better signal-to-noise in the high field studies (the relative NMR sensitivity of ^{195}Pt to ^{1}H is down by 0.00335), we used assemblies of small single crystals with approximate alignment of the b-axis perpendicular to the magnetic field and arbitrary a- and c-axis orientation. This is shown by the highly asymmetric spectral line shape in Figure 12a that is expected to be the combined result of the anisotropic critical field B_c, and hyperfine fields for a randomly-aligned multi-crystalline sample. Most importantly, the spectral amplitude vanishes with increasing temperature in a manner much faster than the conventional Boltzmann 1/T behavior. A similar feature is seen in the magnetic field dependence in Figure 12b, where again the signal vanishes quickly as the upper critical field B_c is reached. We note that attempts to find again a ^{195}Pt line at low temperatures well above 20 T (*i.e.*, 30 T) were unsuccessful. It is possible that until the d-electron spins are fully polarized at much higher fields, the distribution in hyperfine fields at the Pt nuclear site will remain too large to observe an NMR signal.

Figure 11. ^{195}Pt NMR measurements of Per$_2$[Pt(mnt)$_2$]. (**a**) Temperature dependence of $1/T_1$ for 8.56 T and 14 T (polycrystalline sample); (**b**) Angular dependence of ^{195}Pt NMR on a single crystal at 14.774 T and 1.63 K (rotation in a-c plane). The center frequency is 135.16 MHz.

Figure 12. ^{195}Pt spectra of a Per$_2$[Pt(mnt)$_2$] polycrystalline sample. (**a**) Temperature dependence at 14.8 T. Inset: temperature dependence of peak height compared with the 1/T Boltzmann factor; (**b**) Magnetic field dependence at 1.8 K. Traces are offset for clarity; center frequency = $^{195}\gamma$B.

The rapid attenuation of the ^{195}Pt spectral intensity near the SP-CDW phase boundary was the main reason for switching to ^{1}H NMR; this was the only way to probe the SP behavior through the phase transitions. The origin of the ^{195}Pt NMR attenuation may arise from several factors, either in the switching of the hyperfine field to another value far away from the measuring frequency, or by an increasing spatial or temporal fluctuation in the hyperfine field. By inspection Figure 12a,b, it appears that the first moment shifts to lower frequencies as the phase boundary is approached (in T or B), which is consistent with what is seen for ^{1}H NMR. However, since the signal attenuates so quickly, it is difficult to say anything about the line shape and/or the second moment, and spin-relaxation rates become highly uncertain near the phase boundary. If it is assumed that the spectrum of d-electron spin fluctuations is the same for both H and Pt, then the easiest estimate of the ratio of the relaxation rates (at the same temperature and field) at the two sites is their nuclear proximity R to the nearest Pt d-electron spin, *i.e.*,

$$T_1\,(^1H)/T_1(^{195}Pt) \sim R^6(H\text{-}Pt)/R^6(Pt\text{-}Pt) \tag{13}$$
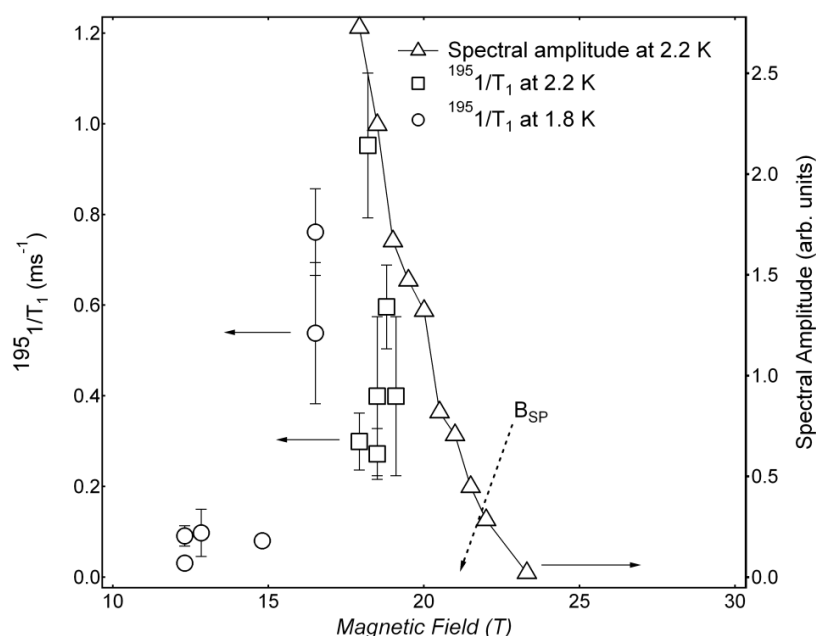
Assuming a nearest neighbor $[1/R^3]^2$ dipolar interaction term between an NMR nucleus and the Pt electronic spin. Comparing a proton at a distance of 10 Å from a Pt electronic spin to a Pt nucleus at a distance of 4 Å from a neighboring Pt electronic spin, the ratio of relaxation rates is only a factor of 240. To get a ratio of order 1000, the effective Pt-Pt distance R (Pt-Pt) would need to be about 3 Å, less than the nearest neighbor Pt-Pt distance of 4.125 Å. This implies that the Pt relaxation and spectra are probably strongly influenced by the hyperfine interactions between each Pt nucleus and its own on-site [Pt(mnt)$_2$]$^-$ spin. Even though the Pt orbital is d-like in symmetry, more than half of its spin density is

distributed over the [Pt(mnt)$_2$]$^-$ anion [24]. We may roughly estimate a lower bound on the hyperfine coupling by considering the shift in the spectral position from 1.74 K to 4.2 K in Figure 12a, using the value for χ at 4.2 K. Here we find $A_{hf} \sim 3700$ Oe/μ_B, again a value significantly higher than that for the proton sites.

A summary of the field dependences of the ^{195}Pt spectral amplitudes and the relaxation rates $1/T_1$ at high magnetic fields near B$_c$ are shown in Figure 13. Although divergences in the relaxation rates may be expected as the phase boundary B$_c$ is approached, the rapidly vanishing signal precluded any definitive determinations. Since the ratio of the relaxation rates of ^{195}Pt to ^{1}H is about 1000, scaling the ^{1}H data in Figure 10b would put $1/T_1 \sim 1.5$ (ms)$^{-1}$ = 1500 s^{-1} at B$_c \sim 20$ T, which seems plausible, base on the range of $1/T_1$ values in Figure 13.

Figure 13. Magnetic field dependence of ^{195}Pt NMR spectral amplitude at 2.2 K and relaxation rates $1/T_1$ at 2.2 and 1.8 K on a Per$_2$[Pt(mnt)$_2$] polycrystalline sample.

6. Experimental Section

All studies were carried out with a standard NMR spectrometer using spin-echo methods. Both superconducting (17 T), resistive (31 T), and Hybrid (45 T) magnets were used with an interchangeable probe that allowed top-tuning and sample rotation in standard helium cryostats. For the ^{1}H measurements, a single crystal (5 × 0.1 × 0.05 mm^3) was used in a micro-coil with an estimated filling factor of 50%. For the ^{1}H studies, the NMR coil was Teflon-coated silver wire, affixed to a Teflon platform on a rotation probe to avoid background proton signals. The long b-axis of the crystal was collinear with the coil, and perpendicular to the magnetic field. Single crystal rotation was in the a-c plane. For the ^{195}Pt measurements, with the exception of one angular dependent study on a single crystal, multiple small crystals were used to enhance the signal-to-noise factor, where only alignment of the b-axis perpendicular to the field was possible, and with no preferred a- or c-axis orientation. A standard insulated copper wire coil was used for these measurements. To validate the simulation code used in Section 3.4, the angular-dependent proton spectrum in the metal-organic framework

$[(CH_3)_2NH_2]Mn(HCOO)_3$ was computed (discarding the disordered $[(CH_3)_2NH_2]$ cation in the center of the framework), agreeing well with an independent simulation in Reference [25].

7. Conclusions

We have used ^1H NMR spectra and spin-relaxation rates ($1/T_1$) to track the behavior of the spin ½ chain in $Per_2[Pt(mnt)_2]$ over a broad range of temperature and magnetic field. Below the spin-Peierls transition ($T < T_c$), the linewidth and $1/T_1$ indicate the formation of a spin-singlet state, but features in magnetic field dependence of the susceptibility and $1/T_1$ show the presence of a minority paramagnetic spin population. These minority spins arise from unpaired spins in the $[Pt(mnt)_2]$ anions, and we find their effects are not observable above 10 T due to the increase in the Zeeman energy. In parallel, for $T < T_c$, with increasing magnetic field the majority spins in the singlet state begin to break down, and the effective spin-Peierls gap decreases. Hence above 10 T, the breaking of the spin chain begins to dominate the behavior of $1/T_1$. Near and above the critical field B_c, we find that the spectra progressively broaden with magnetic field in a manner consistent with the increase in the effective moment μ_{eff} of the dipole interaction, and follow a similar trend seen in torque magnetization studies, and also simulations of ^1H NMR spectra. We estimate it would take about 60 T to fully recover μ_B in the dipole interaction. In contrast, the ^{195}Pt spectra are only observable deep in the SP ground state due to the close proximity of the d-electron moment to the ^{195}Pt nucleus (same atom and nearest neighbor). Hence with increasing temperature, the relaxation rate quickly becomes too fast to measure, and with increasing magnetic field, the breaking of the spin-singlet state creates strong variations in the local hyperfine fields and quickly broadens and shifts the spectral lines.

The signatures of the onset of the SP ground state, based on all NMR spectra and spin relaxation data taken in this study, is that the full SP state appears to form below the CDW transition seen in transport measurements, at least at low magnetic fields. However, at high fields, the two order parameters appear to be coupled more closely. Since NMR is a dynamic probe $\omega \neq 0$, and transport is essentially $\omega = 0$, it is possible that the two methods are affected by different aspects of the transitions as the order parameters develop below T_c. For example, similar differences in apparent phase boundaries have been observed in the case of the field-induced spin density wave phases of $(TMTSF)_2ClO_4$ [26]. Nevertheless, the study presented here is consistent with the notion that the CDW ground state formation is a necessary condition to drive the formation of the SP ground state, and the commensurability of the two order parameter periodicities (2:1) most likely promotes this interaction.

To go beyond the present study, a more detailed investigation of ^1H NMR spectra and $1/T_1$ in the range 20 to 45 T will be needed to resolve features associated with subphases in the high field state. This presents a challenge since GHz range NMR spectroscopy with sufficient power is necessary to overcome the demands on bandwidth due to the increasing linewidths at very high magnetic fields.

Acknowledgments

J.P. Pouget has kindly directed our attention to Figure 5 of his work (Reference [6]) where the inverse structural susceptibility associated with the b*/2 fluctuations is plotted *vs*. temperature. Here, the inverse Curie Weiss-like behavior extrapolates to T_{sp} more clearly than in Figure 2c in the present paper.

Conflict of Interest

The authors declare no conflict of interest.

References

1. Almeida, M.; Henriques, R.T. Perylene based conductors. In *Handbook of Organic Conductive Molecules and Polymers*; Nalwa, H., Ed.; Wiley: New York, NY, USA, 1997; Volume 1, pp. 87–149.

2. Bourbonnais, C.; Henriques, R.T.; Wzietek, P.; Kongeter, D.; Voiron, J.; Jerome, D. Nuclear and electronic resonance approaches to magnetic and lattice fluctuations in the two-chain family of organic compounds (perylene)$_2$[M(S$_2$C$_2$(CN)$_2$)$_2$] (M = Pt, Au). *Phys. Rev.* **1991**, *44*, 641–651.

3. Xavier, J.C.; Pereira, R.G.; Miranda, E.; Affleck, I. Dimerization induced by the RKKY interaction. *Phys. Rev. Lett.* **2003**, *90*, 247204:1–247204:4.

4. Graf, D.; Choi, E.S.; Brooks, J.S.; Matos, M.; Henriques, R.T.; Almeida, M. High magnetic field induced charge density wave state in a quasi-one-dimensional organic conductor. *Phys. Rev. Lett.* **2004**, *93*, 076406:1–076406:4.

5. Green, E.L.; Lumata, L.L.; Brooks, J.S.; Kuhns, P.L.; Reyes, A.P.; Almeida, M.; Matos, M.J.; Henriques, R.T.; Wright, J.A.; Brown, S.E. Interaction of magnetic field-dependent Peierls and spin-Peierls ground states in (Per)$_2$[Pt(mnt)$_2$]. *Phys. Rev.* **2011**, *84*, 121101:1–121101:4.

6. Bonfait, G.; Matos, M.J.; Henriques, R.T.; Almeida, M. Spin-Peierls instability in Per$_2$[M(mnt)$_2$] compounds probed by specific heat. *J. Phys. IV Fr.* **1993**, *3*, C2:251–C2:254.

7. Matos, M.; Bonfait, G.; Henriques, R.T.; Almeida, M. Modification of the magnetic-field dependence of the Peierls transition by a magnetic field. *Phys. Rev.* **1996**, *54*, 15307–15313.

8. Bonfait, G.; Lopes, E.B.; Matos, M.J.; Henriques, R.T.; Almeida, M. Magnetic field dependence of the metal-insulator transition in (Per)$_2$Pt(mnt)$_2$ and (Per)$_2$Au(mnt)$_2$. *Solid State Commun.* **1991**, *80*, 391–394.

9. Gama, V.; Henriques, R.T.; Almeida, M.; Pouget, J.P. Diffuse X-ray scattering evidence for Peierls and "spin-Peierls" like transitions in the organic conductors (Perylene)$_2$[M(mnt)$_2$] (M = Cu, Ni, Co, Fe). *Synth. Met.* **1993**, *55–57*, 1677–1682.

10. Gama, V.; Henriques, R.T.; Almeida, M. *The Series of Organic Conductors (Perylene)$_2$M(mnt)$_2$*; Metzger, R.M., Day, P., Papavassiliou, G., Eds.; Plenum Press: New York, NY, USA, 1991; pp. 205–209.

11. Henriques, R.T.; Alcacer, L.; Pouget, J.P.; Jerome, D. Electrical conductivity and X-ray diffuse scattering study of the family of organic conductors (perylene)$_2$M(mnt)$_2$ (M = Pt, Pd, Au). *J. Phys.* **1984**, *17*, 5197–5208.

12. Alcacer, L.; Novais, H.; Pedroso, F.; Flandrois, S.; Coulon, C.; Chasseau, D.; Gaultier, J. Synthesis, structure and preliminary results on electrical and magnetic properties of (Perylene)$_2$Pt(mnt)$_2$. *Solid State Commun.* **1980**, *35*, 945–949.

13. McDonald, R.D.; Harrison, N.; Balicas, L.; Kim, K.H.; Singleton, J.; Chi, X. Charge-density waves survive the pauli paramagnetic limit. *Phys. Rev. Lett.* **2004**, *93*, 076405:1–076405:4.

14. Graf, D.; Brooks, J.S.; Choi, E.S.; Uji, S.; Dias, J.C.; Almeida, M.; Matos, M. Suppression of a charge density wave ground state in high magnetic fields: Spin and orbital mechanisms. *Phys. Rev.* **2004**, *69*, 125113:1–125113:6.

15. Lumata, L.L. Spin Dynamics of Density Wave and Frustrated Spin Systems Probed by Nuclear Magnetic Resonance. Ph.D. Dissertation, Physics Department, Florida State University, Tallahassee, FL, USA, 2008.

16. Green, E. Magnetic Field Dependent Properties of the Spin-Peierls Chain in the Organic Conductor $Per_2Pt[mnt]_2$. Ph.D. Dissertation, Physics Department, Florida State University, Tallahassee, FL, USA, 2012.

17. Alcácer, L.; Novais, H.; Pedroso, F. *Perylene-Dithiolate Complexes*: *The Platinum Salt*; Plenum Press: New York, NY, USA, 1979; pp. 415–418.

18. Fagot-Revurat, Y.; Horvatic, M.; Berthier, C.; Boucher, J.P.; Segransan, P.; Dhalenne, G.; Revcolevschi, A. ^{63,65}Cu NMR investigation of $CuGeO_3$ single crystals: The uniform and the dimerized spin-Peierls phase. *Phys. Rev.* **1997**, *55*, 2964–2974.

19. Brown, S.E.; Clark, W.G.; Alavi, B.; Hall, D.; Naughton, M.J.; Tantillo, D.J.; Merlic, C.A. High-field magnetization of the spin-Peierls compound $(TMTTF)_2PF_6$. *Phys. Rev.* **1999**, *60*, 6270–6272.

20. Kittel, C. *Introduction to Solid State Physics*, 7th ed.; Wiley: New York, NY, USA, 1996.

21. Maris, G.A. Structural Transitions Induced by Charge and Orbital Ordering in Transition Metal Oxides. Ph.D. Dissertation, Rijksuniversiteit Groningen, Groningen, The Netherlands, 2004.

22. Lemmens, P.; Choi, K.Y.; Valentí, R.; Saha-Dasgupta, T.; Abel, E.; Lee, Y.S.; Chou, F.C. Spin gap formation in the quantum spin systems TiOX, X = Cl and Br. *New J. Phys.* **2005**, *7*, doi:10.1088/1367-2630/7/1/074.

23. Henriques, R.T.; Acacer, L.; Almeida, M.; Tomic, S. Transport and magnetic properties on the family of perylene-dithiolate conductors. *Mol. Cryst. Liq. Cryst.* **1985**, *120*, 237–241.

24. Novoa, J. Department of Quimica Fisica & IQTCUB, Faculty of Quimica, University of Barcelona, Barcelona, Spain. Private Communication, 2011.

25. Besara, T. NMR Near Ferroelectric, Magnetic, and Quantum Phase Transitions. Ph.D. Dissertation, Department Chemistry and Biochemistry and Department of Physics, Florida State University, Tallahassee, FL, USA, 2011.

26. Lumata, L.L.; Brooks, J.S.; Kuhns, P.L.; Reyes, A.P.; Brown, S.E.; Cui, H.B.; Haddon, R. ^{77}Se NMR investigation of the field-induced spin-density-wave transitions in $(TMTSF)_2ClO_4$. *Phys. Rev.* **2008**, *78*, 020407:1–020407:4.